


## Spatial spread of epidemic with Allee effect

Evgeniy Khain \*

*Department of Physics, Oakland University, Rochester, Michigan 48309, USA*

 (Received 11 December 2022; accepted 19 May 2023; published 5 June 2023)

The spatial spread of an epidemic is investigated in the case of a bistable dynamics, where the effective transmission rate depends on the fraction of infected and the state of no epidemic is linearly stable. The front propagation phenomenon is investigated both numerically and theoretically, by an analysis in a four-dimensional phase plane. A good agreement between numerical and theoretical results has been found both for the front profiles and for the speed of invasion. We discovered a novel phenomenon of front stoppage: In some regime of parameters, the front solution ceases to exist, and the propagating pulse of infection decays despite the initial outbreak.

DOI: [10.1103/PhysRevE.107.064303](https://doi.org/10.1103/PhysRevE.107.064303)

### I. INTRODUCTION

In the susceptible-infectious-recovered (SIR) model [1],  $S$  denotes the fraction of susceptible individuals,  $I$  denotes the fraction of infected individuals (people who are sick and can infect others), and  $R$  denotes the fraction of recovered individuals. In the basic model, the initial state of no infection ( $S = 1, I = 0$ ) is unstable if the transmission rate is larger than the recovery rate [1]. Indeed, any small perturbation of this state (when some individuals become infected) leads to an outbreak. In the spatial setting, this may result in fronts propagating into an unstable (healthy) state [2]. In simple cases of reaction-diffusion models that do not consider complex mobility patterns [3], these fronts are qualitatively similar to fronts in the Fisher-Kolmogorov equation [4,5].

Health administrations can effectively fight the epidemic in its initial stages, when the fraction of infected is not large. A common method is tracing the chains of infections [6] and possibly quarantining people who were in a close contact with infected individuals. This method might be quite efficient leading to a reduction in the effective transmission rate; thus it might stabilize the state of no infection to small perturbations. In population dynamics, this phenomenon is called an Allee effect [7], and it was recently proposed to be an important factor in the spread of an epidemic [8]. Mathematically, the effect can be incorporated by introducing the dependence of the transmission rate on the fraction of infected  $I$ , such that the local outbreak occurs only if the initial value of  $I$  is large enough. As a result, the possible traveling wave of infection is qualitatively different from the Fisher-Kolmogorov fronts.

Generally, when two stable states are spatially coupled by diffusion, fronts (for example, density fronts in the insect outbreak model [9]) can propagate in both directions, so either one of the states can win and occupy the entire system [10]. The case of an epidemic is different as without diffusion,  $S$  can only decrease. Therefore, a front can poten-

tially move only in one direction, invading the healthy  $S = 1$  state. Reference [8] analyzed the dynamics of an epidemic in a single well-mixed system. The present research is devoted to a novel phenomenon of spatial epidemic propagation in the SIR model with the Allee effect. Combining numerical and analytical tools, we determine the speed of front propagation and discover the threshold phenomenon, beyond which an initially propagating wave of an epidemic stops.

### II. THE MODEL

The spatial SIR model is usually described by the following reaction-diffusion equations for the fraction of susceptible individuals  $S(x, t)$ , the fraction of infected individuals  $I(x, t)$ , and the fraction of recovered individuals  $R(x, t)$  [1],

$$\begin{aligned}\frac{\partial S}{\partial t} &= -rSI + D\frac{\partial^2 S}{\partial x^2}, \\ \frac{\partial I}{\partial t} &= rSI - \alpha I + D\frac{\partial^2 I}{\partial x^2}, \\ \frac{\partial R}{\partial t} &= \alpha I + D\frac{\partial^2 R}{\partial x^2}.\end{aligned}\quad (1)$$

The equations are accompanied by no-flux boundary conditions. We bring a novel element: While the recovery rate  $\alpha$  is constant, the transmission rate  $r$  depends on the fraction of infected, varying from  $r_{\min} < \alpha$  for low  $I$  ( $I \ll I_{\text{bar}}$ ) to  $r_{\max} > \alpha$  for high  $I$  ( $I \gg I_{\text{bar}}$ ). This can be modeled as

$$r(I) = r_{\min} + (r_{\max} - r_{\min})\frac{I}{I_{\text{bar}} + I}.\quad (2)$$

In this case, both the state of no epidemic  $S = 1, I = 0$  and the final state after the epidemic,  $S = S_{\text{final}}, I = 0$  are stable. In the next section, we study fronts invading the healthy  $S = 1$  state. It turns out, however, that in some regime of parameters, despite the initial outbreak, the front stops moving in finite time, in some sense giving a win to the uninfected  $S = 1$  state.

\*khain@oakland.edu

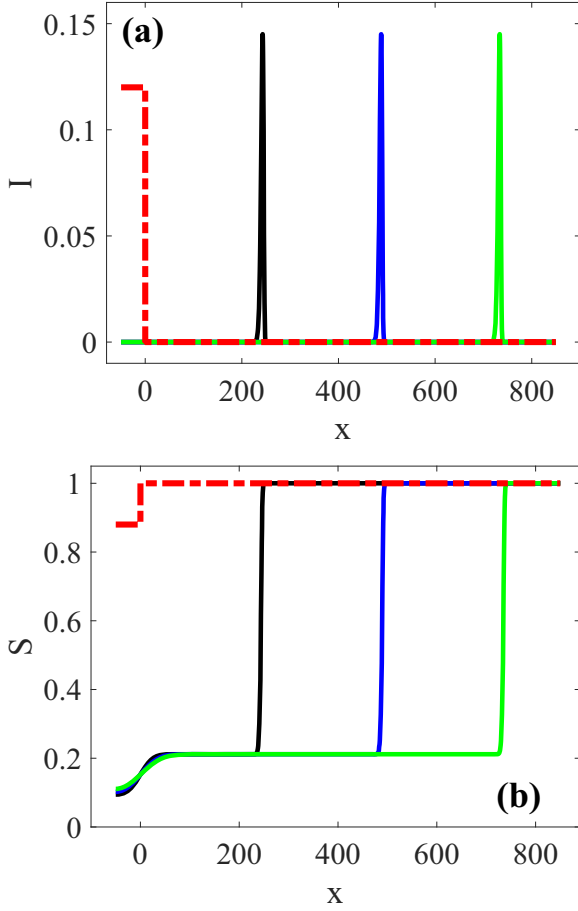


FIG. 1. Spatial profiles of the fraction of infected individuals (the upper panel) and the fraction of susceptible individuals (the lower panel) at different time instances. The curves were computed by numerically solving the system of Eqs. (1). After a short transient, a front propagation is established. In both panels, the profiles are shown at time instances of  $\bar{t} = 0$  (red dashed-dotted curves),  $\bar{t} = 200$  (black curves),  $\bar{t} = 400$  (blue curves), and  $\bar{t} = 600$  (green curves), where  $\bar{t} = \alpha t$  is the rescaled time. The parameters are  $I_{\text{bar}} = 0.02$ ,  $\bar{r}_{\text{min}} = 0.14$ ,  $\bar{r}_{\text{max}} = 2.8$ ,  $D = 1$ , where  $\bar{r}_{\text{min}} = r_{\text{min}}/\alpha$  and  $\bar{r}_{\text{max}} = r_{\text{max}}/\alpha$ .

### III. FRONT PROPAGATION

To study front propagation, it is sufficient to focus just on the first two equations in Eqs. (1). A numerical solution of Eqs. (1) shows that after a short transient, the profiles of  $S$  and  $I$  stop changing with time and start moving with a constant speed  $c$  (see Fig. 1). The upper panel of Fig. 1 shows the profiles of the fraction of infected,  $I$  (the propagating pulse of infection), while the lower panel presents the profiles of the fraction of susceptible,  $S$ . The initial conditions (shown by the red dashed-dotted lines) were chosen to have a form of a step function, where  $I(x, t = 0) = I_0$  in a certain region, and  $I(x, t = 0) = 0$  otherwise. We have checked that the front shape and the speed of propagation do not depend on the value of  $I_0$ , once it is above the threshold for local outbreak. To compute the front speed, we followed the position of the maximum of infected as a function of time. Figure 2 shows that the front speed slowly decreases with

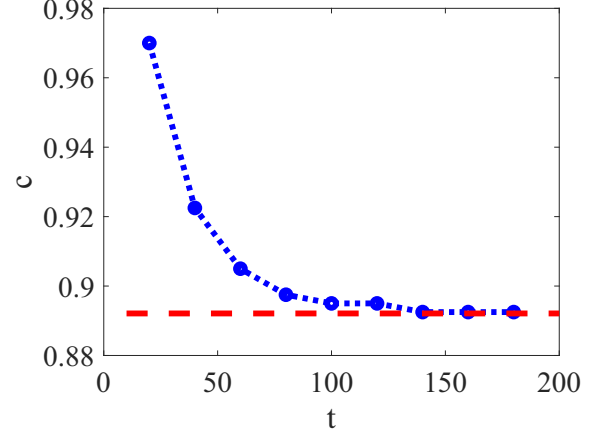


FIG. 2. Front speed computed numerically by solving the system of Eqs. (1) (the blue dotted line) for  $I_{\text{bar}} = 0.025$  (the rest of the parameters are the same as in Fig. 1). The plateau value of the front speed (shown by the red dashed line) is computed theoretically by finding the desired trajectory in a 4D phase space (see text).

time and reaches a plateau that can be determined theoretically (see below).

To make theoretical progress, we first nondimensionalize Eqs. (1), introducing the rescaled dimensionless coordinate  $\bar{x} = \sqrt{D/\alpha}x$  and the rescaled dimensionless time  $\bar{t} = \alpha t$ . Then we substitute the front propagation ansatz, assuming that  $I$  and  $S$  do not separately depend on the coordinate  $\bar{x}$  and time  $\bar{t}$ , but rather on the combination  $\xi = \bar{x} - c\bar{t}$ . Below are the two resulting ordinary differential equations for  $S$  and  $I$ ,

$$-c \frac{dS}{d\xi} = -\bar{r}SI + \frac{d^2S}{d\xi^2}, \quad -c \frac{dI}{d\xi} = \bar{r}SI - I + \frac{d^2I}{d\xi^2}, \quad (3)$$

where  $\bar{r}(I) = r(I)/\alpha$ . Equations (3) can be rewritten as a four-dimensional (4D) dynamical system so that the desired front profile becomes a trajectory in the four-dimensional phase space  $(S, u = dS/d\xi, I, v = dI/d\xi)$ . This trajectory connects the state before the epidemic ( $S = 1, u = 0, I = 0, v = 0$ ) with the state after the epidemic ( $S = S_{\text{final}}, u = 0, I = 0, v = 0$ ). Finding the desired trajectory is challenging since the values of both  $S_{\text{final}}$  and  $c$  are unknown *a priori*. To make progress, we need to theoretically examine the system dynamics near the two states and then employ a so-called “shooting” numerical procedure. Linearizing the system of four first-order differential equations, we obtain

$$\begin{aligned} \frac{d(\delta S)}{d\xi} &= u, & \frac{du}{d\xi} &= -cu + \bar{r}_{\text{min}}S_*I, \\ \frac{dI}{d\xi} &= v, & \frac{dv}{d\xi} &= -cv - \bar{r}_{\text{min}}S_*I + I, \end{aligned} \quad (4)$$

where  $\delta S = S - S_*$ , and  $S_* = S_{\text{final}}$  (when considering the state left behind the front) or  $S_* = 1$  (when considering the state the front propagates to).

First, we analyze the behavior of  $I$  and  $S$  near the  $(S = S_{\text{final}}, I = 0)$  fixed point. Demanding that  $S$  approaches  $S_{\text{final}}$  and  $I$  approaches 0 as  $\xi$  tends to minus infinity, we find the approximate solution in the vicinity of the  $(S = S_{\text{final}}, I = 0)$

state,

$$S(\xi) = S_{\text{final}} + \bar{d} \frac{\bar{r}_{\text{min}} S_{\text{final}}}{(c + \lambda_+) (\lambda_+)^2} \exp(\lambda_+ \xi)$$

and

$$I(\xi) = \frac{\bar{d}}{\lambda_+} \exp(\lambda_+ \xi),$$

where  $\bar{d}$  is an arbitrary (small) constant and the relevant eigenvalue is

$$\lambda_+ = -c/2 + \sqrt{c^2/4 + 1 - \bar{r}_{\text{min}} S_{\text{final}}}.$$

Next, we study the behavior of  $I$  and  $S$  near the  $(S = 1, I = 0)$  fixed point. Linearizing the equations, we again obtain four eigenvalues. Demanding that  $S$  approaches 1 and  $I$  approaches 0 as  $\xi$  tends to plus infinity, we find the approximate solution in the vicinity of the  $(S = 1, I = 0)$  state,

$$S(\xi) = 1 + \bar{a} \frac{\bar{r}_{\text{min}}}{(c + \lambda_-) (\lambda_-)^2} \exp(\lambda_- \xi) + \bar{b} \exp(-c\xi)$$

and

$$I(\xi) = \frac{\bar{a}}{\lambda_-} \exp \lambda_- \xi,$$

where  $\bar{a}$  and  $\bar{b}$  are arbitrary (small) constants and the two relevant eigenvalues are  $\lambda = -c$  and

$$\lambda_- = -c/2 - \sqrt{c^2/4 + 1 - \bar{r}_{\text{min}}}.$$

Since the second term in the expression for  $S$  decays exponentially faster than the last term and can be neglected, the asymptotic approach of  $S$  and  $I$  to the fixed point occurs with different exponents:  $v/I$  approaches  $\lambda_-$  and  $u/(1-S)$  approaches  $c$  as  $\xi \rightarrow \infty$ . To find the trajectory, we perform “shooting” in two parameters:  $c$  and  $S_{\text{final}}$ . We choose a certain interval  $-l_1 < \xi < l_2$ , guess the values of the two parameters, start at  $\xi = l_1$ , solve the dynamical system of equations in MATLAB, and compute  $v/I$  and  $u/(1-S)$  at  $\xi = l_2$ . Performing iterations, we find the values of  $c$  and  $S_{\text{final}}$  that produce the desired behavior of  $v/I$ ,  $u/(1-S)$ . We repeat this procedure for larger and larger intervals (larger  $l_1$  and  $l_2$ ) until the values of  $c$  and  $S_{\text{final}}$  become independent of the chosen interval.

Figure 3 presents an example of such trajectory in two phase planes: The  $(I, v = dI/d\xi)$  phase plane is shown in the upper panel and the  $(S, u = dS/d\xi)$  phase plane in the lower panel. Let us focus first on the trajectory shown by solid line (in both panels). Figure 4 shows this semitheoretical solution of Eqs. (3) and compares it to the numerical solution of Eqs. (1) at large times. An excellent agreement is achieved for the fraction of infected profile (the upper panel) and the fraction of susceptible profile (the lower panel). However, Fig. 3 also presents another solution of Eqs. (3), a different trajectory for the same values of parameters, which is shown by the black dashed lines. We have checked that this trajectory is unstable by choosing the corresponding front profiles as initial conditions  $I(x, t = 0)$  and  $S(x, t = 0)$  for the full system of Eqs. (1). Also, for any other initial conditions, after a transient, the system reached front profiles corresponding to the stable trajectory (blue solid lines in Fig. 3).

To explore the space of parameters, we performed the “shooting” procedure for different values of  $I_{\text{bar}}$  and the

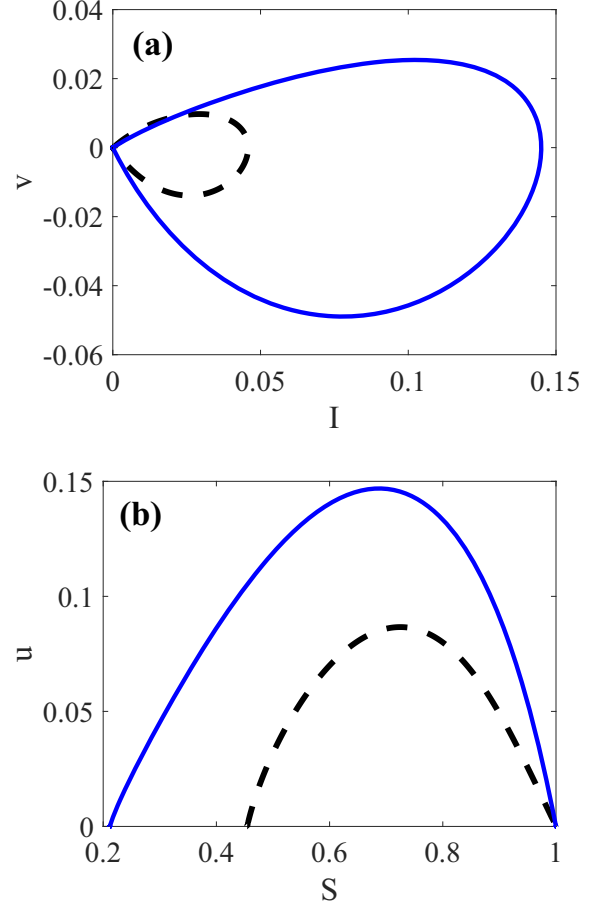


FIG. 3. The trajectory in the phase space of  $I$ ,  $v$  (the upper panel) and  $S$ ,  $u$  (the lower panel) corresponding to the front profiles  $I(\xi)$  and  $S(\xi)$ . The theoretical analysis of the four-dimensional phase space shows two different solutions (two different trajectories in the phase space) for the front propagation problem formulated in Eqs. (3). One of these trajectories is chosen by the dynamics (blue solid curves), i.e., realized as a late time solution of Eqs. (1) (see Fig. 4); another trajectory is unstable and not chosen by the dynamics (black dashed curves). The parameters are the same as in Fig. 1.

rescaled maximal transmission rate  $\bar{r}_{\text{max}}$ . Figure 5 presents the resulting front speed  $c$  and the final fraction of susceptible  $S_{\text{final}}$  as a function of  $I_{\text{bar}}$  for two values of  $\bar{r}_{\text{max}}$ . For the same value of  $I_{\text{bar}}$ , fronts move faster and the outbreak is stronger ( $S_{\text{final}}$  is smaller) for larger  $\bar{r}_{\text{max}}$ . In addition, one can see two intriguing details. First, as discussed above, there are two allowed trajectories for small  $I_{\text{bar}}$ . These two trajectories correspond to different sets of  $(c, S_{\text{final}})$  but only one of these trajectories is stable and chosen by the dynamics as discussed in Fig. 3. More interestingly, the front speed cannot be found for  $I_{\text{bar}}$  larger than some threshold value  $I_{\text{bar},c}$  (the “shooting” procedure is not successful as all the relevant trajectories end up with  $S > 1$ ). Figure 5 shows that the value of  $I_{\text{bar},c}$  depends on  $\bar{r}_{\text{max}}$  (it should also depend on  $\bar{r}_{\text{min}}$ ).

Since there exists no front propagation solution of Eqs. (3) for  $I_{\text{bar}} > I_{\text{bar},c}$ , we examined the behavior of the system in this case by numerically solving Eqs. (1). Figure 6 shows a series of profiles of the fraction of infected at different time

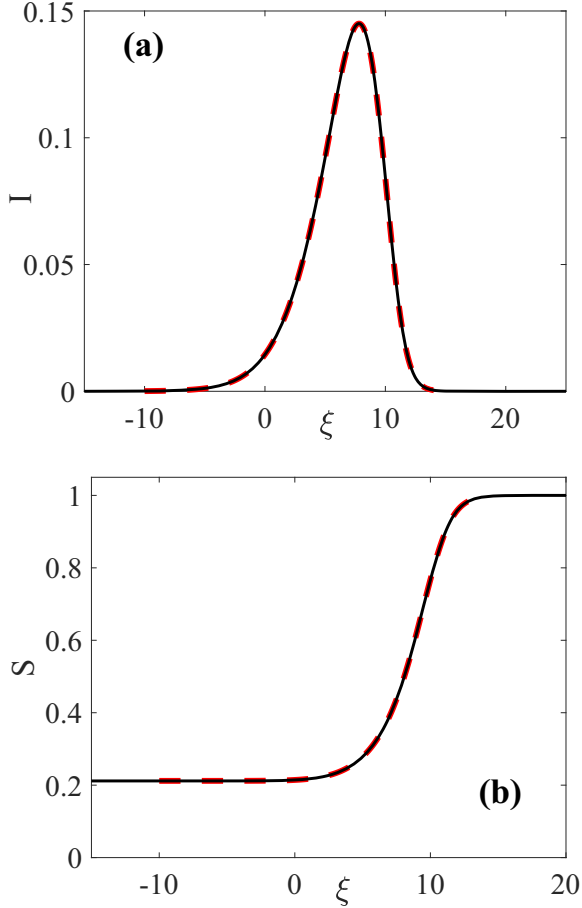


FIG. 4. Front profiles computed both by solving numerically the full system of Eqs. (1) and from the theoretical analysis in the phase space, where the system of Eqs. (3) is solved by using the so-called “shooting” procedure. The numerical solution of Eqs. (1) at late times ( $\bar{t} = 600$ , see Fig. 1) shown by the black solid lines agrees well with the theoretical profiles [solution of Eqs. (3), the red dashed lines] both for the fraction of infected (the upper panel) and the fraction of susceptible (the lower panel). The parameters are the same as in Fig. 1.

instances. First, a large pulse of infected is formed and starts propagating. However, its peak and its speed slowly decrease with time. Eventually, the decrease becomes more dramatic and the pulse completely disappears in final time.

Figure 7 shows the inverse time  $1/t_f$  until the final decay of the pulse as a function of  $Ibar$ . For  $Ibar < Ibar_c$ , the pulse does not decay, so  $t_f$  is infinite and  $1/t_f$  equals zero. This remains true at the threshold value of  $Ibar$ ,  $Ibar_c = 0.025\ 080\ 4$  (computed using the “shooting” procedure). This implies that the threshold value of  $Ibar$  does not depend on initial conditions, and the same conclusion comes from the numerical solution of Eqs. (1) (we varied  $I_0$  from 0.03 to 0.70 and checked that our results do not depend on  $I_0$ ). Interestingly, numerical data points for  $Ibar > Ibar_c$  (circles in Fig. 7) can be fitted by  $1/t_f \propto (Ibar - Ibar_c)^{1/2}$ . Finally, the observed threshold phenomenon does not depend on the diffusion coefficient. For larger  $D$ , the pulse of infection moves a larger distance, but the decay time  $t_f$  remains the same.

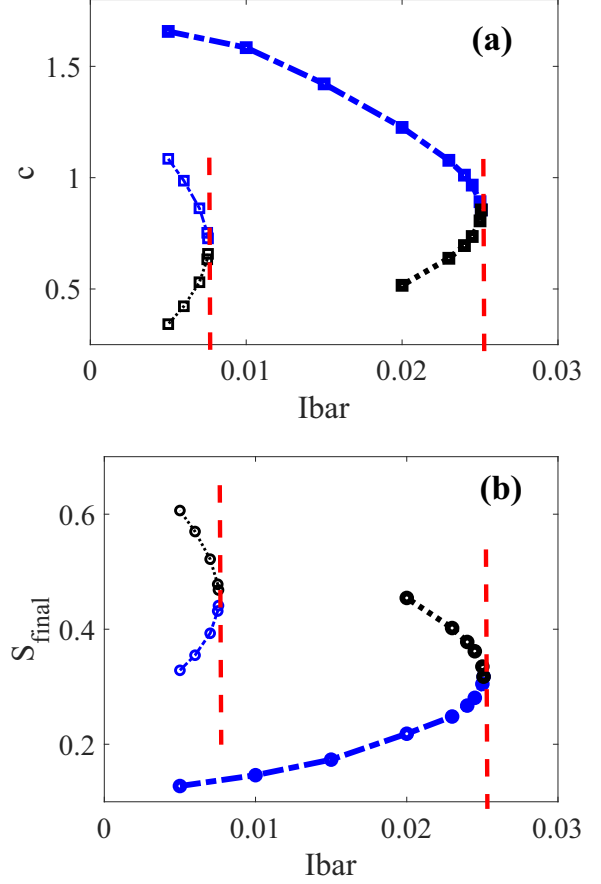


FIG. 5. Front speed (the upper panel) and  $S_{final}$  (the lower panel) computed theoretically as a function of  $Ibar$ . The left curves correspond to  $\bar{r}_{max} = 2.0$ , while the curves on the right correspond to  $\bar{r}_{max} = 2.8$ . Each curve consists of two branches. The blue dashed-dotted lines correspond to the stable branches chosen by the dynamics, while the black dotted lines correspond to the unrealized (unstable) branches (see Fig. 3). There is no front propagation beyond a certain value of  $Ibar$  (the threshold  $I = Ibar_c$  is shown by the red dashed line). The other parameters are the same as in Fig. 1.

IV. SUMMARY AND DISCUSSION

In this paper, we considered the spatial spread of an epidemic in the case of a strong Allee effect, when the “healthy” state  $S = 1, I = 0$  is linearly stable. To model this effect, the transmission rate was assumed to depend on the fraction of infected [8]. We investigated the front propagation phenomenon and computed the speed of the infection wave both numerically and theoretically. We have also discovered a threshold phenomenon of front stoppage: In some regime of parameters, after an initial outbreak, a pulse of infection stops spreading and decays in finite time. Notice that without the Allee effect (in the limit of zero  $Ibar$ ), the wave of infection is qualitatively similar to fronts in the Fisher-Kolmogorov equation, invading the unstable state. Such waves will always propagate, which emphasizes the importance of public health measures (such as tracing the chains of infections) that result in the Allee effect. In other words, even if these health measures do not significantly affect the local epidemiological situation, they might lead (for large enough  $Ibar$ ) to a dramatic global change

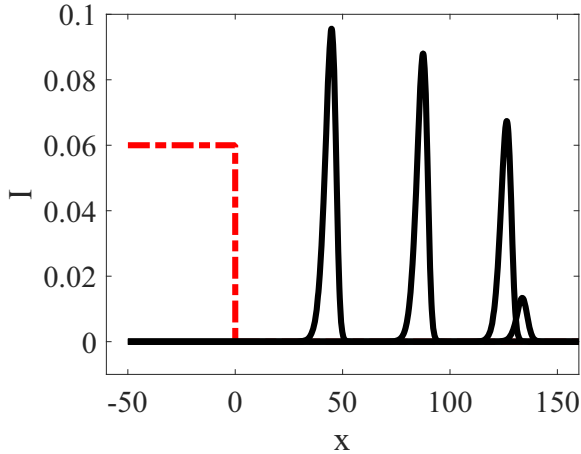


FIG. 6. Fraction of infected profiles at times  $\bar{t} = 0$  (red dashed-dotted curve),  $\bar{t} = 50$ ,  $\bar{t} = 100$ ,  $\bar{t} = 150$ , and  $\bar{t} = 164$  (black solid curves) for  $I_{bar} > I_{bar_c}$  as computed numerically by solving the full system of Eqs. (1).  $I_{bar} = 0.0252$ , and the rest of the parameters are the same as in Fig. 1.

resulting in an eventual stoppage of the propagating pulse of infection.

Interestingly, the observed front propagation is qualitatively different from the well-known phenomenon of a front invading a stable state. In the latter case of a competition between two stable states, a front can move in both directions, and the sign of front speed is determined by the so-called area rule [10]. In our system, the front can move only in one direction, but in some regime of parameters, it gradually stops propagating and the pulse of infection decays. A similar feature for the two systems is that both the area rule and the threshold front stoppage phenomenon are solely determined by the local dynamics and do not depend on the diffusion coefficient.

This paper focuses on front propagation into a metastable state in the deterministic system, but fluctuations might play an important role [11] leading to front wandering and a correction to the front velocity. In our case, fluctuations might affect the critical value of  $I_{bar}$ . As the result, in the vicinity of the threshold the front might still propagate in the deterministic system, but will not move in the stochastic system or vice versa, somewhat similar to the effect examined in Ref. [9].

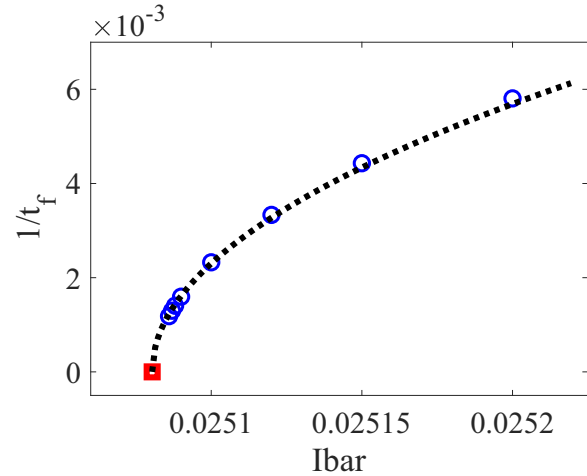


FIG. 7. Inverse pulse decay time as a function of  $I_{bar}$  for  $I_{bar} > I_{bar_c}$  as computed numerically by solving the full system of Eqs. (1) (the blue circles). At the threshold (the red square), the front still propagates, making  $t_f$  infinite, so the inverse decay time is zero. The fit shown by the black dotted line corresponds to  $1/t_f = 0.52 (I_{bar} - I_{bar_c})^{1/2}$ . The rest of the parameters are the same as in Fig. 1.

Investigating this phenomenon is an interesting next step in research. In general, however, the effect of fluctuations should tend to zero as the size of the single-site population increases, therefore, we expect the obtained results to be robust with respect to noise.

Finally, when describing the spread of an epidemic, networks of social contacts represent a more adequate and realistic framework [12] when compared to the continuum well-mixed models, where each person has the same chance of getting infected. We have recently analyzed the front propagation phenomenon in a spatial system of networks interacting by migration [13], considering the standard SIR dynamics. In that case, the front propagates into an unstable state, therefore, the front speed is determined by the linearized dynamics, which greatly simplifies the analysis. Considering a similar setting with a nonlinear bistable SIR dynamics presents a substantial challenge and provides an interesting avenue of future research. We expect the front stoppage phenomenon to be found in that system as well, but the threshold  $I_{bar_c}$  will likely depend on the properties of the node degree distribution.

[1] J. D. Murray, *Mathematical Biology* (Springer, New York, 2002).  
 [2] W. van Saarloos, *Phys. Rep.* **386**, 29 (2003).  
 [3] E. Hanert, E. Schumacher, and E. Deleersnijder, *J. Theor. Biol.* **279**, 9 (2011).  
 [4] R. A. Fisher, *Ann. Eugen.* **7**, 355 (1937).  
 [5] A. N. Kolmogorov, I. G. Petrovsky, and N. S. Piskunov, *Bull. Moscow State Univ. Ser. A: Math. Mech* **1**, 1 (1937).  
 [6] C. Luo, Y. Ma, P. Jiang, T. Zhang, and F. Yin, *Sci. Rep.* **11**, 8605 (2021); R. L. Stuart, W. Zhu, E. F. Morand, and A. Strippa, *Infect. Dis. Health* **26**, 118 (2021).

[7] W. C. Allee and E. Bowen, *J. Exp. Zool.* **61**, 185 (1932); F. Courchamp, J. Berec, and J. Gascoigne, *Allee Effects in Ecology and Conservation* (Oxford University Press, New York, 2008).  
 [8] M. Arim, D. Herrera-Esposito, P. Bermolen, Á. Cabana, M. I. Fariello, M. Lima, and H. Romeroa, *J. Theor. Biol.* **542**, 111109 (2022).  
 [9] E. Khain, Y. T. Lin, and L. M. Sander, *Europhys. Lett.* **93**, 28001 (2011).  
 [10] A. S. Mikhailov, *Foundations of Synergetics: I. Distributed Active Systems* (Springer, Berlin, 1990); J. S. Langer, *Solids Far*

- From Equilibrium*, edited by C. Godreche (Cambridge University Press, Cambridge, UK, 1992).
- [11] B. Meerson, P. V. Sasorov, and Y. Kaplan, *Phys. Rev. E* **84**, 011147 (2011); E. Khain and B. Meerson, *J. Phys. A: Math. Theor.* **46**, 125002 (2013).
- [12] M. J. Keeling and K. T. D. Eames, *J. R. Soc., Interface* **2**, 295 (2005); R. Pastor-Satorras, C. Castellano, P. Van Mieghem, and A. Vespignani, *Rev. Mod. Phys.* **87**, 925 (2015); M. E. J. Newman, *Networks*, 2nd ed. (Oxford University Press, Oxford, UK, 2018).
- [13] E. Khain and M. Iyengar, *Phys. Rev. E* **107**, 034309 (2023).